

Supramolecular Perylene Bisimide-Polysulfide Gel Networks as Nanostructured Redox Mediators in Dissolved Polysulfide Lithium–Sulfur Batteries

Peter D. Frischmann,[†] Laura C. H. Gerber,[†] Sean E. Doris,^{†,⊥} Erica Y. Tsai,[†] Frank Y. Fan,[‡] Xiaohui Qu,[§] Anubhav Jain,[§] Kristin A. Persson,[§] Yet-Ming Chiang,[‡] and Brett A. Helms^{*,†}

[†]The Molecular Foundry, Lawrence Berkeley National Laboratory, One Cyclotron Road, Berkeley, California 94720, United States

[⊥]Department of Chemistry, University of California, Berkeley, California 94720, United States

[‡]Department of Materials Science and Engineering, Massachusetts Institute of Technology, Cambridge, Massachusetts 02139, United States

[§]Computational Research Division, Lawrence Berkeley National Laboratory, One Cyclotron Road, Berkeley, California 94720, United States

Supporting Information

ABSTRACT: Here we report a new redox-active perylene bisimide (PBI)-polysulfide (PS) gel that overcomes electronic charge-transport bottlenecks common to lithium–sulfur (Li–S) hybrid redox flow batteries designed for long-duration grid-scale energy storage applications. PBI was identified as a supramolecular redox mediator for soluble lithium polysulfides from a library of 85 polycyclic aromatic hydrocarbons by using a high-throughput computational platform; furthermore, these theoretical predictions were validated electrochemically. Challenging conventional wisdom, we found that π -stacked PBI assemblies were stable even in their reduced state through secondary interactions between PBI nanofibers and Li_2S_n , which resulted in a redox-active, flowable 3-D gel network. The influence of supramolecular charge-transporting PBI-PS gel networks on Li–S battery performance was investigated in depth and revealed enhanced sulfur utilization and rate performance (C/4 and C/8) at a sulfur loading of 4 mg cm^{-2} and energy density of 44 Wh L^{-1} in the absence of conductive carbon additives.



INTRODUCTION

A renaissance in electrochemical energy storage is underway, fueled both by demand and by the burgeoning field of nanotechnology.^{1,2} Within this context, organic and polymeric nanomaterials are gaining prominence for their ability to impart novel functions in energy storage devices—including self-healing character,³ overcharge protection,⁴ and adaptive charge transport.⁵ The modular character and the precision with which they can be prepared continue to advance our understanding of structure–property relationships in polymer electrolytes,^{6,7} ion-selective membranes and separators,^{8,9} charge-storage materials,^{10–15} and binders.⁵ Enhancing charge transport in devices by exerting control over component architectures across multiple length scales remains an outstanding challenge in the field.

Here we advance supramolecular design principles^{16–18} for the programmed self-assembly of π -conjugated molecules that enable us to coassemble molecular redox mediators and charge-storing inorganic materials into flowable, redox-active 3-D gels. To showcase our nanostructured redox mediator concept, we have investigated the charge-transporting properties of these soft supramolecular gels in lithium–sulfur (Li–S) batteries (Figure 1a). Related organogels composed of molecular semiconductors assembled into nanofiber morphologies^{19–21}

have shown interesting properties for electrical conductivity,^{22–24} electroluminescence,²⁵ colorimetric sensing,²⁶ photo-induced charge separation,²⁷ light-harvesting,²⁸ and photosensitization of H_2 -evolving catalysts.²⁹ Nonetheless, the application of organic π -gelators in electrochemical energy storage is unexplored.

Our focus on Li–S batteries as a test-bed for this concept is tied to their potential to deliver low-cost, energy-dense storage that is scalable for both transportation and grid-scale applications.³⁰ Nevertheless, persistent hurdles to commercialization of Li–S batteries remain. For example, a well-known polysulfide (PS) shuttle reaction, where soluble Li_2S_n ($n = 4, 6,$ and 8) cross the separator and react with the Li-metal anode, contributes to a short cycle life.^{31,32} Creative solutions addressing PS crossover in solid-state Li–S secondary cells have focused on trapping PS within nanostructured scaffolds.^{33–37} In parallel, interest in dissolved PS catholytes is rapidly growing,^{38–41} where high PS solubility and fast reaction kinetics are advantageous to battery performance. The

Received: July 31, 2015

Revised: September 15, 2015

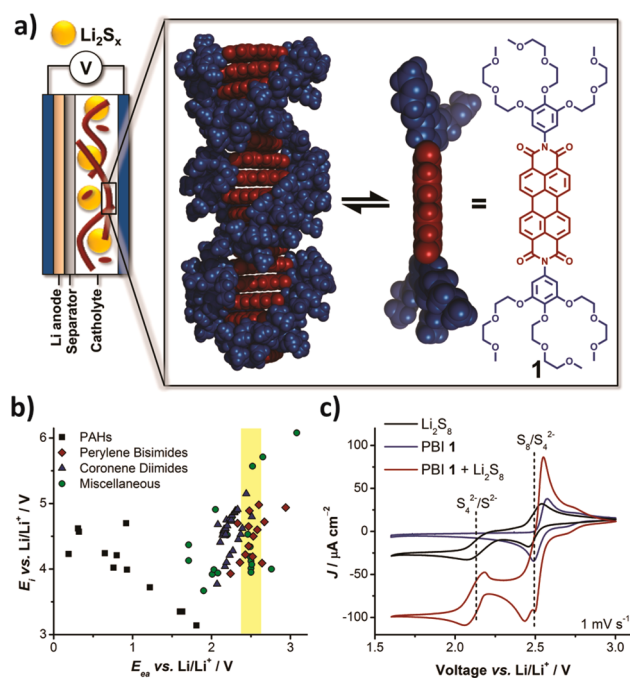


Figure 1. a) Li–S cell diagram of nanostructured PBI 1-PS catholyte with side-on view of the PBI π -surface and its self-assembly into 1-D nanowires through π -stacking. b) Plot of E_i vs. E_{ca} calculated for candidate π -gelators. The yellow bar highlights the voltage window of interest for matching the calculated E_{ca} of the redox mediator to the S_8/S_4^{2-} redox couple. c) Cyclic voltammograms of Li_2S_8 , **1**, and **1** + Li_2S_8 in TEGDME with LiTFSI (0.50 mol L⁻¹) and LiNO₃ (0.15 mol L⁻¹) as electrolyte. The concentration of **1** is 0.010 mol L⁻¹ and Li_2S_8 is 0.010 mol S L⁻¹ in all voltammograms.

discovery of LiNO₃ as an anode protecting additive^{42,43} has allowed sulfur catholyte formulations to be optimized for flow battery architectures; for example, the electronic charge transport and sulfur utilization are greatly enhanced using nanocarbon (e.g., Ketjenblack) suspensions as embedded current collectors, which increase the effective surface area of the electrode.^{44,45}

To understand the factors influencing rate performance and sulfur utilization in Li–S cells employing flowable sulfur catholytes, we turned our attention to redox mediators,⁴⁶ and in particular to π -conjugated organic molecules, which can be tailored to lower barrier heights for charge transfer across electrolyte-current collector interfaces. Inspired by the dynamic reconfigurability of the Ketjenblack suspensions in facilitating charge transport in those catholytes, we hypothesized our redox mediators would likewise benefit from a 3-D networked architecture in the electrolyte, which would allow charge transport to proceed via self-exchange along the supramolecular assemblies (i.e., via a hopping mechanism). Our success in this regard lays new foundations for designing flowable electrodes with adaptive charge-transporting and charge-storing properties. These characteristics are desirable for redox flow battery applications (i.e., long-duration, grid-scale energy storage), where the rheology of the network is subject to molecular-level control and where the network can self-heal when disrupted during intermittent flow pulses.⁴⁷ Depending on the redox chemistry of the mediator, there are further opportunities to halt electron transport at the voltage extrema used to cycle the battery, thereby offering overcharge or overdischarge protection.

RESULTS AND DISCUSSION

Design Criteria of Supramolecular Redox Mediator and Electrochemical Validation of the High-Throughput Computational Platform. Two principal design criteria were considered in search of a redox-active π -gelator tailored for operation in a Li–S battery: 1) the redox chemistry of the molecular π -gelator needs to match with the charge/discharge potential of a Li–S battery (~ 2.5 V vs Li/Li⁺ for dissolved PS) to enable charge transport during cycling; and 2) to maintain pathways for electronic percolation, the molecular structure of the mediator must provide sustainable noncovalent interactions for nanowire formation at various states of charge that are not disrupted by high salt or PS concentrations.

To accelerate materials discovery with respect to the first design criterion, we developed a high-throughput computational platform to screen π -gelator candidates based on electron affinity (E_{ca}) and ionization potential (E_i).^{48,49} A mixed density functional theory and polarizable continuum model approach was applied to address geometry optimization, solvation free energy, and electronic energy in a dielectric continuum medium. The screened molecular library spanned several classes of organogelators, and the wide distribution of calculated E_i vs. E_{ca} emphasizes the value of the high-throughput platform in streamlining the materials discovery process (Figure 1b and Table S1).

As a proof of concept demonstration, we focused on the 2.5 V soluble long-chain PS redox couple attributed to $S_8 \rightarrow Li_2S_4$ to avoid complicating phase transformations associated with precipitation of insulating Li_2S .^{31,32} Precipitation of active material is a well-known driver of capacity fade in redox flow batteries, and increased cycle life and power have been achieved by limiting discharge to the soluble long-chain PS regime.^{39,40} Of the 85 structures screened (Figures 1b and S1–S2), perylene bisimide (PBI) emerged as a leading candidate due to its calculated $E_{ca} = 2.53$ V vs Li/Li⁺ closely matching the S_8/S_4^{2-} redox couple. In addition, PBIs are an established class of n-type semiconductor known for self-assembly into π -stacks, reversible redox chemistry, and synthetic accessibility—all desired features for a supramolecular redox mediator.^{50,51}

With respect to the second design criterion, PBI **1** was designed and synthesized to serve as a redox mediator capable of assembling into extended supramolecular networks to help facilitate charge transport in soluble PS catholytes (Figure 1a, synthetic details found in the SI). The oligo-ethylene glycol imide substituents of **1** impart solubility in electrolyte while maintaining a π -surface accessible for π -stacking.

Our high-throughput computational platform predicted an E_{ca} value of 2.47 V vs Li/Li⁺ for a model compound closely related to **1** (PBI **1** in Figure S2). We validated the theoretical prediction by measuring cyclic voltammograms of **1** in tetraethylene glycol dimethyl ether (TEGDME) with lithium bis(trifluoromethanesulfonyl)imide (LiTFSI) and LiNO₃ as supporting electrolyte. A reversible redox wave was observed at 2.53 V vs Li/Li⁺ (Figures 1c and S4), confirming the accuracy of the calculations to within 60 mV and establishing **1** as electrochemically active in the range of soluble PS.

Comparing cyclic voltammograms of **1**, Li_2S_8 , and **1** + Li_2S_8 (Figure 1c) confirms that **1** serves as a redox mediator for soluble long-chain PS. The two redox waves for Li_2S_8 centered at 2.5 and 2.1 V are attributed to the processes $S_8 \rightarrow S_4^{2-}$ and $S_4^{2-} \rightarrow S_2^{2-}$, respectively.^{52–54} Introduction of **1** to the Li_2S_8 solution results in a 4-fold increase in current density at the 2.5

V redox wave, roughly twice the summation of the PS and PBI I redox couples measured in isolation. This provides evidence that **1** is serving as a redox mediator for increased charge transfer to and from long-chain PS species in solution.

Characterization of PBI Self-Assembly and PBI-PS Gel Morphology. To verify that **1** assembles into nanostructured redox mediators in battery electrolyte, the self-assembly of **1** was studied by UV-vis spectroscopy in TEGDME containing 0.50 mol L⁻¹ LiTFSI. PBI **1** exhibited dramatic spectroscopic changes as the concentration was increased from 1.4 × 10⁻⁶ to 1.5 × 10⁻³ mol L⁻¹ due to π -stacking into extended nanowire aggregates (Figure 2a).^{50,51} The increase in optical density

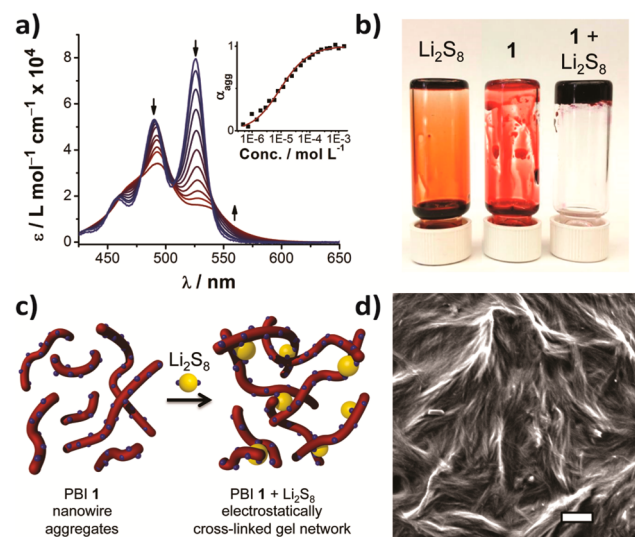


Figure 2. a) Concentration dependent UV-vis spectra of PBI **1** in electrolyte. Arrows indicate changes with increasing concentration. Inset: nonlinear curve fitting of the concentration series at $\lambda = 555$ nm (expressed as the degree of aggregation α_{agg}) to an isodesmic self-assembly model yielding $K_a = 6.1 \times 10^4$ L mol⁻¹. b) Picture of Li₂S₈, **1**, and **1** + Li₂S₈ in electrolyte, showing unique gelation behavior for **1** + Li₂S₈. c) Electrostatic cross-linking of the nanowire aggregates is triggered by addition of Li₂S₈ resulting in a gel with high local concentration of PS immobilized on the redox mediator network. d) Xerogel of the nanofiber network formed from **1** + Li₂S₈ (scale bar is 1 μ m).

above 550 nm with increasing concentration was used to quantify the strength of self-assembly. Fitting the spectroscopic changes to an isodesmic self-assembly model yielded an association constant of $K_a = 6.1 \pm 0.3 \times 10^4$ L mol⁻¹. From this determination of K_a , number (N) and weight (N_w) average aggregate sizes of 55 and 108, respectively, are calculated for a 0.048 mol L⁻¹ solution of **1**. Based on N , N_w , a typical π -stacking distance of 0.35 nm, and the 3.1 nm end-to-end length of **1**, an average cylindrical primary aggregate size of 20–40 nm in length by 3 nm in diameter was estimated.

Catholyte solutions containing 2.5 mol S L⁻¹ as Li₂S₈ and 0.048 mol L⁻¹ PBI (5.0% w/w) in TEGDME with LiTFSI (0.50 mol L⁻¹) and LiNO₃ (0.15 mol L⁻¹) were prepared. Despite extensive aggregation of **1** in electrolyte, it remained highly soluble, and no gelation was observed. Within 5 min of mixing **1** with Li₂S₈ a deep purple gel developed and then remained soft but stable to inversion. A picture of Li₂S₈, **1**, and **1** + Li₂S₈ in electrolyte depicts the unique rheology of the **1** + Li₂S₈ catholyte (Figure 2b), and a video highlighting the flowability of the catholyte gel is included with the SI. The color change

distinguishing solutions of **1** from **1** + Li₂S₈ is due to partial PBI reduction by Li₂S₈. This reduction is fully reversible upon exposure to air, which was tracked by UV-vis spectroscopy (Figure S5).

Our hypothesis for the mechanism of gelation is outlined in Figure 2c. PBI **1** exists in electrolyte as long supramolecular nanofibers coated in a Li⁺ sheath, where Li⁺ interacts with the side chains of **1**. Upon introduction of S₈²⁻, weakly associated TFSI⁻ counterions are displaced and the divalent PS act as electrostatic cross-links, weaving nanowires of **1** into a continuous fabric (Figure 2d). This cross-linking effectively increases the local concentration of active material in contact with the redox mediator network and may facilitate interchain electron transfer between PBI nanowires. To estimate the strength of the cross-linking reaction $2[\text{1} \cdot \text{LiTFSI}] + \text{Li}_2\text{S}_8 \rightleftharpoons [\text{1} \cdot \text{Li}_2\text{S}_8 \cdot \text{1}] + 2[\text{LiTFSI}]$ the equilibrium constant was calculated to be $K_{\text{eq}} = 64$ using a mixed density functional theory and polarizable continuum model approach (see the SI for details). The energetically favorable cross-linking and potential density of cross-linking interactions (roughly 6:1 S₈²⁻:PBI molar ratio) drives gelation of the PBI-PS network.

The unique nanoscale morphology of **1** + Li₂S₈ was apparent in scanning electron micrographs of dried xerogels, which showed fibrous networks spanning tens of microns (Figures 2d and S6). Although additional aggregation is expected upon evaporation of solvent, the large association constant, quantified by UV-vis spectroscopy, supports that similar networked assemblies are present prior to solvent evaporation. We anticipated that these networks of redox mediators colocalized with PS would provide new opportunities to mediate charge transfer in Li-S cells.

Supramolecular Redox Mediators in Li-S Cells.

Electrochemical testing of Li-S secondary cells (Swagelok type) was carried out using Li metal anodes, porous polymer separators, and flowable PBI-PS gel catholytes. Cells were galvanostatically cycled from 2.8 to 2.0 V in the S₈ → S₄²⁻ regime where 1C rate is defined as the reaction of 0.5 equiv of Li⁺ with 1 equiv of sulfur per hour (theoretical capacity of 418 mAh g⁻¹ S).^{39,40} The catholyte composition was 2.5 mol S L⁻¹ as Li₂S₈ (sulfur loading of ~4 mg cm⁻²) with 5.0% w/w PBI **1** when applicable. Charge/discharge curves at a C/8 rate showed a discharge plateau for the S₈ → S₈²⁻ reaction, followed by a gradual sloping regime for the S₈²⁻ → S₄²⁻ reaction (Figure 3a). Discharge capacities of 267 ± 6 and 193 ± 11 mAh g⁻¹ (S) for **1** + Li₂S₈ and Li₂S₈, respectively, were measured (Tables S2 and S3). A 38% increase in sulfur utilization was observed with the nanostructured **1** + Li₂S₈ gel network compared to Li₂S₈ alone. Supramolecular catholyte **1** + Li₂S₈ exhibits a volumetric energy density of 44 Wh L⁻¹, exceeding the industry standard of 25–40 Wh L⁻¹ observed for advanced aqueous vanadium redox-flow technology.⁵⁵ Although PBI is a known Li-ion storage material,^{56–58} capacities below 5 mAh g⁻¹ were measured for **1** in the absence of Li₂S₈ at similar current densities, indicating that **1** does not contribute significantly to the overall capacity.

Enhanced sulfur utilization at C/8, C/4, and C/2 rates was observed for the nanostructured **1** + Li₂S₈ gel catholyte, whereas at 1C rate both catholytes showed nearly equivalent performance. Both catholytes showed rate tolerance, recovering their initial C/8 rate capacity after cycling at higher current densities up to 1C (Figure 3b). Stable cycling with an average 99% capacity retention per cycle was observed for the **1** + Li₂S₈ gel catholyte and Li₂S₈ alone after 20 cycles (Figure 3c). Coulombic efficiencies increased with cycle number from 68–

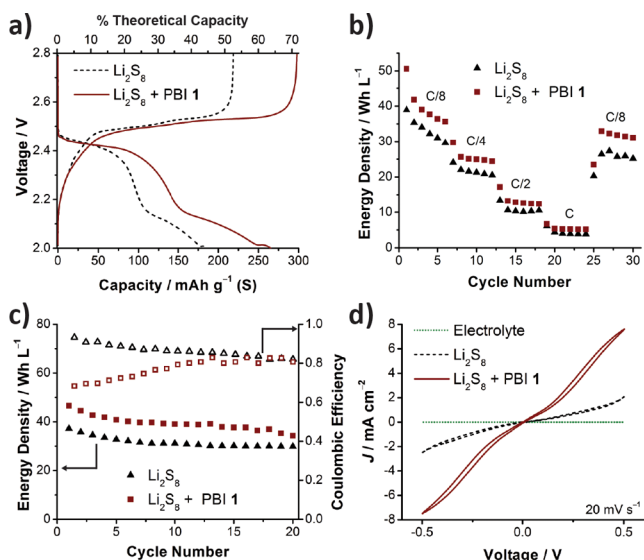


Figure 3. a) Charge–discharge profiles from galvanostatic cycling (second cycle) at a C/8 rate showing a 38% increase in discharge capacity for PBI 1 + Li_2S_8 . b) Rate performance at C/8, C/4, C/2, and 1C. c) Energy density (solid) and Coulombic efficiency (hollow) vs. cycle number at C/8 rate. d) IV curves from cyclic voltammetry with an interdigitated array electrode.

81% for **1** + Li_2S_8 , and decreasing Coulombic efficiencies of 93–82% were measured for Li_2S_8 alone. Lower Coulombic efficiencies are expected due to increased PS shuttling in the absence of an ion-selective membrane or physical PS trap, especially because the 2.8–2.0 V operating voltage lies mostly in the soluble PS regime. Combining the supramolecular PBI redox mediator network with PS trapping strategies may enable extended cycling studies in the future.

Additional evidence relating these performance improvements with the **1** + Li_2S_8 catholyte gel to increased redox shuttling current was obtained from IV curves of catholyte measured with an interdigitated array electrode by sweeping a ± 0.5 V bias from the open circuit potential at a scan rate of 20 mV s^{-1} (Figure 3d). Introduction of 10 mol % **1** relative to sulfur resulted in a 300% increase in the shuttling current at a 0.5 V bias for **1** + Li_2S_8 relative to Li_2S_8 alone. The mechanism of charge transport through self-assembled nanofibers is under further investigation; however, we hypothesize that rapid self-exchange of electrons through π -stacks of PBI nanowires, as has been previously reported,⁵⁹ is partially responsible for the increased current. Related self-assembled nanowires of π -stacked hexabenzocoronenes have also shown enhanced solution-state electron transport when chemically doped.⁶⁰

Having successfully demonstrated our proof of concept for a charge-transporting PBI redox mediator network, improved rate performance was further achieved by including conductive carbon cloth (C-cloth) with the dissolved PBI-PS gel catholyte. By analogy to biological vasculature, charge transport in these cells propagates through both “arteries” and “capillaries”: that is to say, current travels from the electrode surface through the 8 μm diameter C-cloth arteries and then is locally distributed to PS by the nanoscale PBI capillary network. Galvanostatic charge–discharge curves are depicted in Figure 4a highlighting a clear performance improvement in both capacity and overpotential for C-cloth + Li_2S_8 + PBI **1** compared to the C-cloth + Li_2S_8 control without redox mediator. Discharge capacities of 328 ± 19 and $250 \pm 17 \text{ mAh g}^{-1}$ (S) were

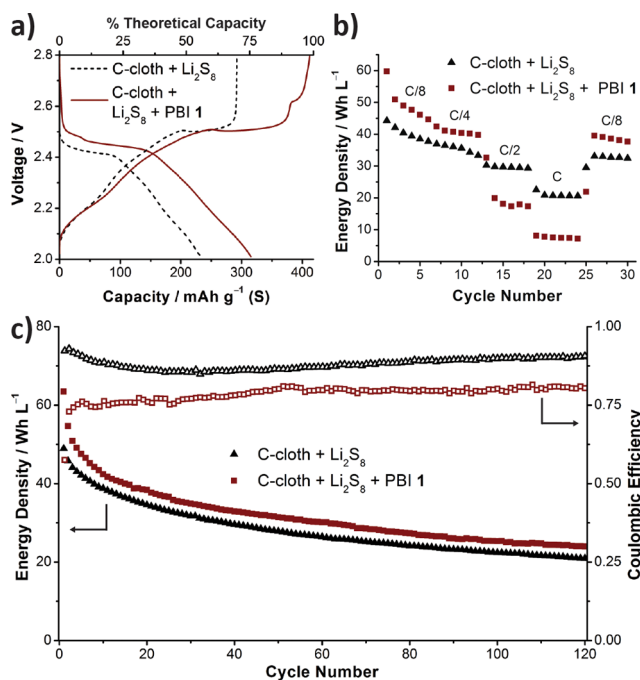


Figure 4. a) Charge–discharge profiles from galvanostatic cycling (second cycle) at a C/8 rate showing a 31% increase in discharge capacity for C-cloth + Li_2S_8 + PBI **1**. b) Rate performance at C/8, C/4, C/2, and 1C. c) Energy density (solid) and Coulombic efficiency (hollow) vs. cycle number at C/4 rate.

measured for C-cloth + Li_2S_8 + PBI **1** and C-cloth + Li_2S_8 alone, respectively, representing a 31% increase in sulfur utilization attributed to the redox mediator network.

Interestingly, the “arteries and capillaries” network exhibits a clear advantage over the control at C/8 and C/4 rates (Figure 4b), but at C/2 and 1C rates the trend is reversed. A caveat for this observation relates to the increased viscosity of the PBI-PS gel network impeding ion transport at higher current densities. Higher electrolyte resistance was measured for PBI-PS gel catholytes by electrochemical impedance spectroscopy (EIS) of Li–S cells at open circuit potential, and ionic conductivities of 0.007 S cm^{-2} and 0.02 S cm^{-2} were calculated for PBI-PS gel and PS alone, respectively (Figure S7). Because electronic conductivity was rate limiting in the absence of C-cloth, this trend was not observed in Figure 3b. Although high power batteries are desired for electric vehicles and frequency regulation, flow batteries are most useful for long duration grid-storage applications like load shifting and peak shaving, where a 4–8 h discharge time (i.e., at C/4 to C/8 rate) is ideal.

Both C-cloth + Li_2S_8 + PBI **1** and C-cloth + Li_2S_8 alone exhibit a 99% capacity retention per cycle averaged over 120 cycles at C/4 rate as depicted in Figure 4c. As in the case of the C-cloth free cells, lower Coulombic efficiency is measured for the catholyte containing PBI redox mediator. The fact that the lower Coulombic efficiency does not contribute to faster capacity fade suggests that the reduced efficiency results from the PBI redox mediator reversibly shuttling charge across the mesoporous separator. A microporous PS- and PBI-blocking separator may be applied in the future to minimize shuttling and increase energy efficiency of supramolecular gel network catholytes.⁶¹

CONCLUSIONS

In summary, supramolecular gel networks of π -stacked redox mediators improve sulfur utilization and rate performance of Li–S batteries, even in the absence of any conductive carbons. To our knowledge, this discovery is the first demonstration of a nanostructured yet flowable PS-organogel catholyte for electrochemical energy storage. A high-throughput computational platform was developed to rapidly screen candidate π -gelators by E_{ca} and E_i to ensure redox activity at relevant Li–S potentials. PBI was identified as a redox mediator for the soluble PS regime, and a new PBI derivative was designed that self-assembles into nanofiber networks with PS under highly reducing conditions in electrolyte. Even in this early demonstration, these supramolecular gel catholytes deliver a volumetric energy density of 44 Wh L⁻¹ at sulfur loadings of 4 mg cm⁻². The reconfigurable nature of self-assembled nanowire gels is a promising feature for transitioning this discovery to redox flow architectures for long-duration grid-scale energy storage applications. Efforts to increase order in self-assembled nanowires for rapid charge-transport and tune the chemical potential for operation at the 2.0 V Li₂S precipitation plateau are ongoing.

ASSOCIATED CONTENT

Supporting Information

The Supporting Information is available free of charge on the ACS Publications website at DOI: 10.1021/acs.chemmater.5b02955.

Synthesis and characterization, computational details, UV–vis, CV, and SEM (PDF)
Video of a flowing PBI-PS gel (MPG)

AUTHOR INFORMATION

Corresponding Author

*E-mail: BAHelms@lbl.gov.

Notes

The authors declare no competing financial interest.

ACKNOWLEDGMENTS

This work was supported by the Joint Center for Energy Storage Research, an Energy Innovation Hub funded by the U.S. Department of Energy, Office of Science, Office of Basic Energy Sciences. Portions of the work were carried out as a user project at the Molecular Foundry, which is supported by the Office of Science, Office of Basic Energy Sciences, of the U.S. Department of Energy under contract no. DE-AC02-05CH11231. This research used resources of the National Energy Research Scientific Computing Center, a DOE Office of Science User Facility supported by the Office of Science of the U.S. Department of Energy under Contract No. DE-AC02-05CH11231. S.E.D. was supported by the Department of Defense through the National Defense Science & Engineering Graduate Fellowship Program. E.Y.T. acknowledges support from the DOE Science Undergraduate Laboratory Internship program. We acknowledge T. E. Williams for SEM assistance.

REFERENCES

- (1) Goodenough, J. B. Electrochemical Energy Storage in a Sustainable Modern Society. *Energy Environ. Sci.* **2014**, *7*, 14–18.
- (2) Bruce, P. G.; Freunberger, S. A.; Hardwick, L. J.; Tarascon, J.-M. Li–O₂ and Li–S Batteries with High Energy Storage. *Nat. Mater.* **2012**, *11*, 19–29.

- (3) Wang, C.; Wu, H.; Chen, Z.; McDowell, M. T.; Cui, Y.; Bao, Z. Self-healing Chemistry Enables the Stable Operation of Silicon Microparticle Anodes for High-energy Lithium-ion Batteries. *Nat. Chem.* **2013**, *5*, 1042–1048.

- (4) Wang, B.; Richardson, T. J.; Chen, G. Electroactive Polymer Fiber Separators for Stable and Reversible Overcharge Protection in Rechargeable Lithium Batteries. *J. Electrochem. Soc.* **2014**, *161*, A1039–A1044.

- (5) Wu, M.; Xiao, X.; Vukmirovic, N.; Xun, S.; Das, P. K.; Song, X.; Olalde-Velasco, P.; Wang, D.; Weber, A. Z.; Wang, L.-W.; Battaglia, V. S.; Yang, W.; Liu, G. Toward an Ideal Polymer Binder Design for High-Capacity Battery Anodes. *J. Am. Chem. Soc.* **2013**, *135*, 12048–12056.

- (6) Bouchet, R.; Maria, S.; Meziane, R.; Aboulaich, A.; Lienafa, L.; Bonnet, J.-P.; Phan, T. N. T.; Bertin, D.; Gimes, D.; Devaux, D.; Denoyel, R.; Armand, M. Single-ion BAB Triblock Copolymers as Highly Efficient Electrolytes for Lithium-metal Batteries. *Nat. Mater.* **2013**, *12*, 452–457.

- (7) Javier, A. E.; Patel, S. N.; Hallinan, D. T., Jr.; Srinivasan, V.; Balsara, N. P. Simultaneous Electronic and Ionic Conduction in a Block Copolymer: Application in Lithium Battery Electrodes. *Angew. Chem., Int. Ed.* **2011**, *50*, 9848–9851.

- (8) Kumar, B. V. V. S. P.; Rao, K. V.; Sampath, S.; George, S. J.; Eswaramoorthy, M. Supramolecular Gating of Ion Transport in Nanochannels. *Angew. Chem., Int. Ed.* **2014**, *53*, 13073–13077.

- (9) Xu, T.; Zhao, N.; Ren, F.; Hourani, R.; Lee, M. T.; Shu, J. Y.; Mao, S.; Helms, B. A. Subnanometer Porous Thin Films by the Co-assembly of Nanotube Subunits and Block Copolymers. *ACS Nano* **2011**, *5*, 1376–1384.

- (10) Liang, Y.; Tao, Z.; Chen, J. Organic Electrode Materials for Rechargeable Lithium Batteries. *Adv. Energy Mater.* **2012**, *2*, 742–769.

- (11) Huskinson, B.; Marshak, M. P.; Suh, C.; Er, S.; Gerhardt, M. R.; Galvin, C. J.; Chen, X.; Aspuru-Guzik, A.; Gordon, R. G.; Aziz, M. J. A Metal-free Organic-inorganic Aqueous Flow Battery. *Nature* **2014**, *505*, 195–198.

- (12) Nagarjuna, G.; Hui, J.; Cheng, K. J.; Lichtenstein, T.; Shen, M.; Moore, J. S.; Rodríguez-López, J. Impact of Redox-Active Polymer Molecular Weight on the Electrochemical Properties and Transport Across Porous Separators in Nonaqueous Solvents. *J. Am. Chem. Soc.* **2014**, *136*, 16309–16316.

- (13) Simmonds, A. G.; Griebel, J. J.; Park, J.; Kim, K. R.; Chung, W. J.; Oleshko, V. P.; Kim, J.; Kim, E. T.; Glass, R. S.; Soles, C. L.; Sung, Y.-E.; Char, K.; Pyun, J. Inverse Vulcanization of Elemental Sulfur to Prepare Polymeric Electrode Materials for Li–S Batteries. *ACS Macro Lett.* **2014**, *3*, 229–232.

- (14) Huang, J.; Cheng, L.; Assary, R. S.; Wang, P.; Xue, Z.; Burrell, A. K.; Curtiss, L. A.; Zhang, L. Liquid Catholyte Molecules for Nonaqueous Redox Flow Batteries. *Adv. Energy Mater.* **2015**, *5*, DOI: 10.1002/aenm.201401782.

- (15) Wei, X.; Xu, W.; Vijayakumar, M.; Cosimbescu, L.; Liu, T.; Sprenkle, V.; Wang, W. TEMPO-Based Catholyte for High-Energy Density Nonaqueous Redox Flow Batteries. *Adv. Mater.* **2014**, *26*, 7649–7653.

- (16) Aida, T.; Meijer, E. W.; Stupp, S. I. Functional Supramolecular Polymers. *Science* **2012**, *335*, 813–817.

- (17) Pisula, W.; Feng, X.; Müllen, K. Tuning the Columnar Organization of Discotic Polycyclic Aromatic Hydrocarbons. *Adv. Mater.* **2010**, *22*, 3634–3649.

- (18) Lehn, J.-M. From Supramolecular Chemistry Towards Constitutional Dynamic Chemistry and Adaptive Chemistry. *Chem. Soc. Rev.* **2007**, *36*, 151–160.

- (19) Babu, S. S.; Praveen, V. K.; Ajayaghosh, A. Functional π -Gelators and Their Applications. *Chem. Rev.* **2014**, *114*, 1973–2129.

- (20) Weiss, R. G. The Past, Present, and Future of Molecular Gels. What Is the Status of the Field, and Where Is It Going? *J. Am. Chem. Soc.* **2014**, *136*, 7519–7530.

- (21) Amabilino, D. B.; Puigmarti-Luis, J. Gels as Soft Matter Route to Conducting Nanostructured Organic and Composite Materials. *Soft Matter* **2010**, *6*, 1605–1612.

- (22) Chen, L.; Mali, K. S.; Puniredd, S. R.; Baumgarten, M.; Parvez, K.; Pisula, W.; De Feyter, S.; Müllen, K. Assembly and Fiber Formation of a Gemini-Type Hexathienocoronene Amphiphile for Electrical Conduction. *J. Am. Chem. Soc.* **2013**, *135*, 13531–13537.
- (23) Kumar, R. J.; MacDonald, J. M.; Singh, T. B.; Waddington, L. J.; Holmes, A. B. Hierarchical Self-Assembly of Semiconductor Functionalized Peptide α -Helices and Optoelectronic Properties. *J. Am. Chem. Soc.* **2011**, *133*, 8564–8573.
- (24) Stone, D. A.; Tayi, A. S.; Goldberger, J. E.; Palmer, L. C.; Stupp, S. I. Self-assembly and Conductivity of Hydrogen-bonded Oligothiophene Nanofiber Networks. *Chem. Commun.* **2011**, *47*, 5702–5704.
- (25) Diring, S.; Camerel, F.; Donnio, B.; Dintzer, T.; Toffanin, S.; Capelli, R.; Muccini, M.; Ziessel, R. Luminescent Ethynyl–Pyrene Liquid Crystals and Gels for Optoelectronic Devices. *J. Am. Chem. Soc.* **2009**, *131*, 18177–18185.
- (26) Mukhopadhyay, P.; Iwashita, Y.; Shirakawa, M.; Kawano, S.; Fujita, N.; Shinkai, S. Spontaneous Colorimetric Sensing of the Positional Isomers of Dihydroxynaphthalene in a 1D Organogel Matrix. *Angew. Chem., Int. Ed.* **2006**, *45*, 1592–1595.
- (27) Sugiyasu, K.; Kawano, S.; Fujita, N.; Shinkai, S. Self-Sorting Organogels with p–n Heterojunction Points. *Chem. Mater.* **2008**, *20*, 2863–2865.
- (28) Würthner, F.; Bauer, C.; Stepanenko, V.; Yagai, S. A Black Perylene Bisimide Super Gelator with an Unexpected J-Type Absorption Band. *Adv. Mater.* **2008**, *20*, 1695–1698.
- (29) Weingarten, A. S.; Kazantsev, R. V.; Palmer, L. C.; McClendon, M.; Koltonow, A. R.; Samuel, A. P. S.; Kiebal, D. J.; Wasielewski, M. R.; Stupp, S. I. Self-assembling Hydrogel Scaffolds for Photocatalytic Hydrogen Production. *Nat. Chem.* **2014**, *6*, 964–970.
- (30) Manthiram, A.; Fu, Y.; Chung, S.-H.; Zu, C.; Su, Y.-S. Rechargeable Lithium–Sulfur Batteries. *Chem. Rev.* **2014**, *114*, 11751–11787.
- (31) Zhang, S. S. Liquid Electrolyte Lithium/Sulfur Battery: Fundamental Chemistry, Problems, and Solutions. *J. Power Sources* **2013**, *231*, 153–162.
- (32) Choi, N.-S.; Chen, Z.; Freunberger, S. A.; Ji, X.; Sun, Y.-K.; Amine, K.; Yushin, G.; Nazar, L. F.; Cho, J.; Bruce, P. G. Challenges Facing Lithium Batteries and Electrical Double-Layer Capacitors. *Angew. Chem., Int. Ed.* **2012**, *51*, 9994–10024.
- (33) Yang, Y.; Zheng, G.; Cui, Y. Nanostructured Sulfur Cathodes. *Chem. Soc. Rev.* **2013**, *42*, 3018–3032.
- (34) Kim, J.; Lee, D.-J.; Jung, H.-G.; Sun, Y.-K.; Hassoun, J.; Scrosati, B. An Advanced Lithium–Sulfur Battery. *Adv. Funct. Mater.* **2013**, *23*, 1076–1080.
- (35) Guo, J.; Yang, Z.; Yu, Y.; Abruña, H. D.; Archer, L. A. Lithium–Sulfur Battery Cathode Enabled by Lithium–Nitrile Interaction. *J. Am. Chem. Soc.* **2013**, *135*, 763–767.
- (36) Song, M.-K.; Zhang, Y.; Cairns, E. J. A Long-Life, High-Rate Lithium/Sulfur Cell: A Multifaceted Approach to Enhancing Cell Performance. *Nano Lett.* **2013**, *13*, 5891–5899.
- (37) Ji, X.; Lee, K. T.; Nazar, L. F. A Highly Ordered Nanostructured Carbon–Sulphur Cathode for Lithium–Sulphur Batteries. *Nat. Mater.* **2009**, *8*, 500–506.
- (38) Pu, X.; Yang, G.; Yu, C. Liquid-Type Cathode Enabled by 3D Sponge-Like Carbon Nanotubes for High Energy Density and Long Cycling Life of Li–S Batteries. *Adv. Mater.* **2014**, *26*, 7456–7461.
- (39) Su, Y.-S.; Fu, Y.; Guo, B.; Dai, S.; Manthiram, A. Fast, Reversible Lithium Storage with a Sulfur/Long-Chain-Polysulfide Redox Couple. *Chem. - Eur. J.* **2013**, *19*, 8621–8626.
- (40) Yang, Y.; Zheng, G.; Cui, Y. A Membrane-free Lithium/Polysulfide Semi-liquid Battery for Large-scale Energy Storage. *Energy Environ. Sci.* **2013**, *6*, 1552–1558.
- (41) Demir-Cakan, R.; Morcrette, M.; Gangulibabu; Guéguen, A.; Dedryvère, R.; Tarascon, J.-M. Li–S Batteries: Simple Approaches for Superior Performance. *Energy Environ. Sci.* **2013**, *6*, 176–182.
- (42) Aurbach, D.; Pollak, E.; Elazari, R.; Salitra, G.; Kelley, C. S.; Affinito, J. On the Surface Chemical Aspects of Very High Energy Density, Rechargeable Li–Sulfur Batteries. *J. Electrochem. Soc.* **2009**, *156*, A694–A702.
- (43) Mikhaylik, Y. V. Electrolytes for Lithium Sulfur Cells. U.S. Pat. US7,354,680, 2008.
- (44) Fan, F. Y.; Woodford, W. H.; Li, Z.; Baram, N.; Smith, K. C.; Helal, A.; McKinley, G. H.; Carter, W. C.; Chiang, Y.-M. Polysulfide Flow Batteries Enabled by Percolating Nanoscale Conductor Networks. *Nano Lett.* **2014**, *14*, 2210–2218.
- (45) Chen, H.; Zou, Q.; Liang, Z.; Liu, H.; Li, Q.; Lu, Y.-C. Sulphur-impregnated Flow Cathode to Enable High-energy-density Lithium Flow Batteries. *Nat. Commun.* **2015**, *6*, 5877.
- (46) The only example of a redox mediator applied to Li–S batteries involved metallocenes to reduce the overpotential of Li₂S cathode activation: Meini, S.; Elazari, R.; Rosenman, A.; Garsuch, A.; Aurbach, D. The Use of Redox Mediators for Enhancing Utilization of Li₂S Cathodes for Advanced Li–S Battery Systems. *J. Phys. Chem. Lett.* **2014**, *5*, 915–918.
- (47) Smith, K. C.; Chiang, Y.-M.; Carter, W. C. Maximizing Energetic Efficiency in Flow Batteries Utilizing Non-Newtonian Fluids. *J. Electrochem. Soc.* **2014**, *161*, A486–A496.
- (48) Cheng, L.; Assary, R. S.; Qu, X.; Jain, A.; Ong, S. P.; Rajput, N. N.; Persson, K.; Curtiss, L. A. Accelerating Electrolyte Discovery for Energy Storage with High-Throughput Screening. *J. Phys. Chem. Lett.* **2015**, *6*, 283–291.
- (49) Qu, X.; Jain, A.; Rajput, N. N.; Cheng, L.; Zhang, Y.; Ong, S. P.; Brafman, M.; Maginn, E.; Curtiss, L. A.; Persson, K. A. The Electrolyte Genome Project: A Big Data Approach in Battery Materials Discovery. *Comput. Mater. Sci.* **2015**, *103*, 56–67.
- (50) Zhan, X.; Facchetti, A.; Barlow, S.; Marks, T. J.; Ratner, M. A.; Wasielewski, M. R.; Marder, S. R. Rylene and Related Diimides for Organic Electronics. *Adv. Mater.* **2011**, *23*, 268–284.
- (51) Würthner, F. Perylene Bisimide Dyes as Versatile Building Blocks for Functional Supramolecular Architectures. *Chem. Commun.* **2004**, 1564–1579.
- (52) Assary, R. S.; Curtiss, L. A.; Moore, J. S. Toward a Molecular Understanding of Energetics in Li–S Batteries Using Nonaqueous Electrolytes: A High-Level Quantum Chemical Study. *J. Phys. Chem. C* **2014**, *118*, 11545–11558.
- (53) Barchasz, C.; Molton, F.; Duboc, C.; Leprêtre, J.-C.; Patoux, S.; Alloin, F. Lithium/Sulfur Cell Discharge Mechanism: An Original Approach for Intermediate Species Identification. *Anal. Chem.* **2012**, *84*, 3973–3980.
- (54) Gao, J.; Lowe, M. A.; Kiya, Y.; Abruña, H. D. Effects of Liquid Electrolytes on the Charge–Discharge Performance of Rechargeable Lithium/Sulfur Batteries: Electrochemical and in-Situ X-ray Absorption Spectroscopic Studies. *J. Phys. Chem. C* **2011**, *115*, 25132–25137.
- (55) Larcher, D.; Tarascon, J.-M. Towards Greener and More Sustainable Batteries for Electrical Energy Storage. *Nat. Chem.* **2015**, *7*, 19–29.
- (56) Tian, D.; Zhang, H.-Z.; Zhang, D.-S.; Chang, Z.; Han, J.; Gao, X.-P.; Bu, X.-H. Li-ion Storage and Gas Adsorption Properties of Porous Polyimides (PIs). *RSC Adv.* **2014**, *4*, 7506–7510.
- (57) Sharma, P.; Damien, D.; Nagarajan, K.; Shaijumon, M. M.; Hariharan, M. Perylene-polyimide-Based Organic Electrode Materials for Rechargeable Lithium Batteries. *J. Phys. Chem. Lett.* **2013**, *4*, 3192–3197.
- (58) Han, X.; Chang, C.; Yuan, L.; Sun, T.; Sun, J. Aromatic Carbonyl Derivative Polymers as High-Performance Li-Ion Storage Materials. *Adv. Mater.* **2007**, *19*, 1616–1621.
- (59) Williams, M. E.; Murray, R. W. Perylene Polyether Hybrids: Highly Soluble, Luminescent, Redox-Active Dyes. *Chem. Mater.* **1998**, *10*, 3603–3610.
- (60) Gerber, L. C. H.; Frischmann, P. D.; Williams, T. E.; Tichelaar, M.; Tsai, E. Y.; Liu, Y.-S.; Guo, J.; Pemmaraju, C. D.; Prendergast, D.; Helms, B. A. Chemical Doping Enhances Electronic Transport in Networks of Hexabenzocoronenes Assembled in Non-aqueous Electrolyte. *Polym. Chem.* **2015**, *6*, 5560–5564.
- (61) Li, C.; Ward, A. L.; Doris, S. E.; Pascal, T. A.; Prendergast, D.; Helms, B. A. A Polysulfide-Blocking Microporous Polymer Membrane Tailored for Hybrid Li–Sulfur Flow Batteries. *Nano Lett.* **2015**, *15*, 5724–5729.